Lack of BACE1 S-palmitoylation reduces amyloid burden and mitigates memory deficits in transgenic mouse models of Alzheimer's disease

Robert J. Andrew[a,b,c,1], Celia G. Fernandez[a,b,c,1], Molly Stanley[d,e], Hong Jiang[d,e], Phuong Nguyen[f], Richard C. Rice[a,b,c], Virginie Buggia-Prévot[a,b,c], Pierre De Rossi[a,b,c], Kulandaivelu S. Vetrivel[a,b,c], Raza Lamb[a,b,c], Arnau Argemi[a,b,c], Emilie S. Allaert[a,b,c], Elle M. Rathbun[a,b,c], Sofia V. Krause[a,b,c], Steven L. Wagner[f], Angèle T. Parent[a,b,c], David M. Holtzman[d,e], and Gopal Thinakaran[a,b,c,2]

[a]Department of Neurobiology, The University of Chicago, Chicago, IL 60637; [b]Department of Neurology, The University of Chicago, Chicago, IL 60637; [c]Department of Pathology, The University of Chicago, Chicago, IL 60637; [d]Hope Center for Neurological Disorders, Department of Neurology, Washington University School of Medicine, St. Louis, MO 63110; [e]Knight Alzheimer's Disease Research Center, Department of Neurology, Washington University School of Medicine, St. Louis, MO 63110; and [f]Department of Neurosciences, University of California, San Diego, La Jolla, CA 92093

Alzheimer's disease (AD) is a devastating neurodegenerative disorder characterized by pathological brain lesions and a decline in cognitive function. β-Amyloid peptides (Aβ), derived from proteolytic processing of amyloid precursor protein (APP), play a central role in AD pathogenesis. β-Site APP cleaving enzyme 1 (BACE1), the transmembrane aspartyl protease which initiates Aβ production, is axonally transported in neurons and accumulates in dystrophic neurites near cerebral amyloid deposits in AD. BACE1 is modified by S-palmitoylation at four juxtamembrane cysteine residues. S-palmitoylation is a dynamic posttranslational modification that is important for trafficking and function of several synaptic proteins. Here, we investigated the in vivo significance of BACE1 S-palmitoylation through the analysis of knock-in mice with cysteine-to-alanine substitution at the palmitoylated residues (4CA mice). BACE1 expression, as well as processing of APP and other neuronal substrates, was unaltered in 4CA mice despite the lack of BACE1 S-palmitoylation and reduced lipid raft association. Whereas steady-state Aβ levels were similar, synaptic activity-induced endogenous Aβ production was not observed in 4CA mice. Furthermore, we report a significant reduction of cerebral amyloid burden and BACE1 accumulation in dystrophic neurites in the absence of BACE1 S-palmitoylation in mouse models of AD amyloidosis. Studies in cultured neurons suggest that S-palmitoylation is required for dendritic spine localization and axonal targeting of BACE1. Finally, the lack of BACE1 S-palmitoylation mitigates cognitive deficits in 5XFAD mice. Using transgenic mouse models, these results demonstrate that intrinsic posttranslational S-palmitoylation of BACE1 has a significant impact on amyloid pathogenesis and the consequent cognitive decline.

neurodegeneration | 5XFAD | PDAPP | axonal transport | dystrophic neurite

Alzheimer's disease (AD) is pathologically characterized by the production and deposition of oligomeric and aggregated forms of β-amyloid peptides (Aβ), which have been implicated in neuronal dysfunction and neuronal cell death. Sequential cleavage of amyloid precursor protein (APP) by β-site cleaving enzyme 1 (BACE1) and γ-secretase generates Aβ (1). Human genetic studies provide compelling evidence for the significance of BACE1 cleavage of APP to the development of AD. Mutations in the residues immediately preceding the BACE1 cleavage site (K670N/M671L) cause familial AD by elevating Aβ production (2–4). Amino acid variations adjacent to the BACE1 cleavage site either increase (A673V) or decrease (A673T) BACE1 processing and Aβ production, thus influencing the risk for AD and cognitive decline (5–7). Since the initial description and characterization of its proteolysis of APP, a plethora of other BACE1 substrates have been identified using candidate approaches and quantitative proteomics (8, 9), several of which have been shown to rely upon proteolysis by

BACE1 for their cellular function. Still, BACE1 inhibitor drugs to target APP proteolysis are being evaluated for their therapeutic potential for AD.

BACE1 undergoes S-palmitoylation at four juxtamembrane cysteine residues (C474, C478, C482, and C485) (10). S-palmitoylation is a reversible posttranslational modification responsible for targeting a variety of peripheral and integral membrane proteins to lipid rafts (also referred to as membrane rafts) in nonneuronal cells and in neurons (11, 12). In addition to lipid raft targeting, S-palmitoylation is a critical modification that dynamically regulates membrane trafficking and modulates the function of proteins such as neuronal transmembrane receptors (AMPA and NMDA receptors) and cytosolic proteins (PSD-95) (13–16). Studies in cultured cell lines showed that S-palmitoylation of BACE1 does not influence the enzymatic processing of APP (10, 17). Nevertheless, cell culture studies are insufficient to capture the complex neuronal regulation of BACE1 dynamics in the brain and the physiological

Significance

Alzheimer's disease (AD) is a devastating neurodegenerative disorder for which no preventative drug or cure is currently available. BACE1 is a key enzyme that initiates the production of β-amyloid peptides (Aβ), which accumulate in AD brain and contribute to cognitive decline. BACE1 undergoes S-palmitoylation, a lipid modification that is known to regulate neuronal protein trafficking. We investigated the in vivo significance of BACE1 S-palmitoylation by generating knock-in mice selectively lacking this modification. The lack of BACE1 S-palmitoylation impaired synaptic activity-induced Aβ production, significantly reduced cerebral amyloid burden in AD mouse models, and mitigated cognitive deficits. Using transgenic mouse models, our results demonstrate that intrinsic posttranslational S-palmitoylation of BACE1 has a significant impact on amyloid pathogenesis and the consequent cognitive decline.

and pathological significance of BACE1 S-palmitoylation in vivo. Therefore, we generated knock-in mice with cysteine-to-alanine substitution at the four residues that are the targets for S-palmitoylation in BACE1 (4CA line) and characterized amyloid pathology by crossing the 4CA line with two transgenic AD mouse models. Here, we report an impairment in the activity-induced increase of Aβ in 4CA mice and a significant decrease in amyloid burden in the brains of AD mouse models expressing S-palmitoylation–deficient BACE1 concomitant with the rescue of behavioral deficits. Moreover, in cultured hippocampal neurons, dendritic spine localization and axonal transport are markedly diminished for BACE1 lacking the sites of S-palmitoylation. Our results are consistent with S-palmitoylation–dependent regulation of neuronal BACE1 trafficking and function that impacts on the extent of AD pathology in the brain.

Results

Generation of Mice Expressing S-Palmitoylation–Deficient BACE1. The 4CA knock-in mice carrying alanine substitution at the four BACE1 S-palmitoylation sites (cysteines 474, 478, 482, and 485) were generated using the strategy outlined in Fig. 1A. Homozygous 4CA animals are viable and appear phenotypically normal. The steady-state levels of BACE1 in the brains of homozygous 4CA mice and wild-type littermates (WT mice) at postnatal day 7 (P7) and P60 were similar (Fig. 1B; and see Fig. S3B). BACE1 S-palmitoylation in WT and 4CA mouse brain was assessed using the acyl-resin assisted capture (acyl-RAC) method (18, 19). Forebrain lysates from P7 mice were incubated with methyl methanethiosulfonate to block free thiols before cleavage of thioester linkages between palmitoylated cysteine residues and fatty-acid palmitate using hydroxylamine. Nascent thiols were subsequently captured on thiopropyl Sepharose and analyzed by immunoblotting. S-palmitoylated BACE1 was recovered in the bound fraction from WT mice. However, 4CA-BACE1, which cannot undergo S-palmitoylation was detected only in the unbound fraction (Fig. 1C). Reprobing of the blots revealed comparable levels of two palmitoylated proteins, PSD95 and Flotillin 2, confirming the successful capture of S-palmitoylated proteins from WT and 4CA brain lysates.

Posttranslational S-palmitoylation is a potential mechanism for regulating raft association of several cytosolic and transmembrane proteins. Therefore, lipid raft distribution of wild-type (wt) BACE1 and 4CA-BACE1 was analyzed by isolating detergent-insoluble membrane microdomains by discontinuous flotation density gradient centrifugation of mouse brain lysates (20). Lubrol WX-resistant buoyant light density membranes, enriched in the classical lipid raft-associated protein Flotillin-2, were found in fractions 4 through 6, at the interface between 5% and 35% sucrose. Consistent with previous reports, we found that a portion of wt BACE1 partitioned into raft fractions with a raft/nonraft distribution similar to that of Flotillin-2. However, the levels of 4CA-BACE1 were markedly lower in the raft fractions and elevated in nonraft fractions (Fig. 1D). Quantitative analysis revealed a significant decrease in the raft/nonraft distribution of 4CA-BACE1 compared with wt BACE1 (Fig. 1E). Further analysis revealed that a fraction of APP was recovered in lipid rafts fractions as expected, but no difference was observed in relative raft distribution of APP between WT and 4CA mice. Thus, the results described above show that 4CA-BACE1 failed to undergo S-palmitoylation, which impaired its lipid raft association in mouse brain.

Proteolytic Processing of APP and Other Neuronal Substrates Is Unaffected by the Lack of BACE1 S-Palmitoylation. In the mouse brain, BACE1 is enriched in the hippocampal mossy fibers (21, 22), and mice lacking BACE1 expression have shortened and disorganized infrapyramidal mossy fiber bundles (21). The localization of wt BACE1 and 4CA-BACE1 in the granule cell axonal projections from the dentate gyrus to CA3 was similar (Fig. S1A). Moreover, analysis of 2-mo-old animals revealed no marked difference in the appearance of the infrapyramidal mossy fiber bundle (IPB) and no quantitative difference in IPB length (Fig. S1B). BACE1 knockout mice also exhibit axon guidance defects in the olfactory bulb, evidenced by malformed glomeruli and mistargeted olfactory sensory axons (23, 24). Immunofluorescence analysis revealed olfactory sensory axon terminal localization of 4CA-BACE1 and no obvious axon misguidance defects or any difference in BACE 1 accumulation in olfactory glomeruli (Fig. S2). These findings indicate that the lack of BACE1 S-palmitoylation
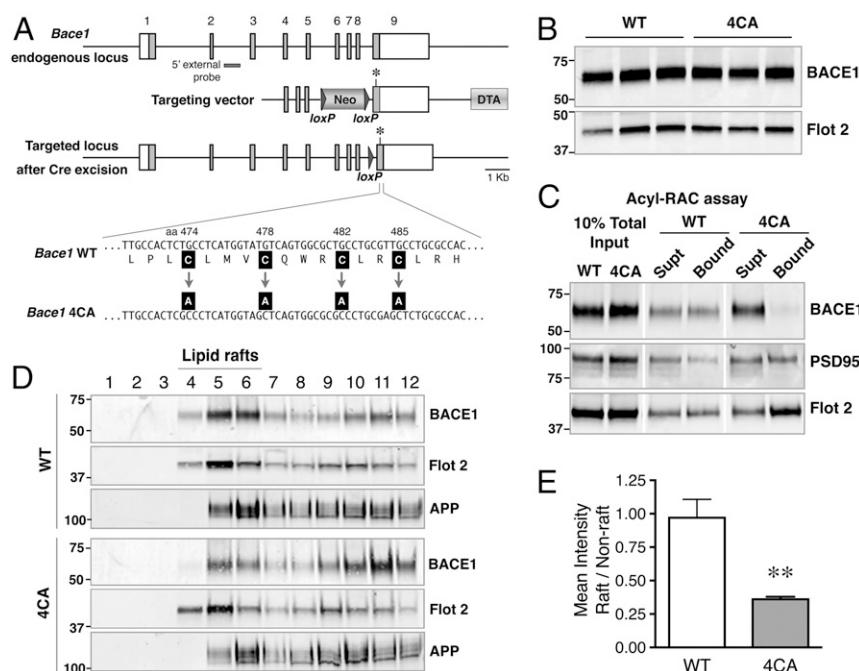

Fig. 1. Generation of 4CA knock-in mice. (A, Top) Schematic representation of the Bace1 locus showing the nine exons (numbered); coding regions are shown as filled gray boxes. (Middle) The homology arms of the targeting vector are shown along with the loxP-flanked PGK-Neo and the Diptheria Toxin A (DTA) selection cassettes. An asterisk indicates a silent mutation introduced to generate a unique SacI site in the mutant allele. (Bottom) Schematic structure of the targeted allele after Cre-mediated excision of the PGK-Neo gene. The cysteine-to-alanine substitutions are indicated. (B) Total brain homogenates of WT and 4CA mice (P7) were analyzed by immunoblotting. (C) Detection of S-palmitoylated BACE1 in mouse brain by acyl-RAC. Mouse brain lysates (P7) were subjected to acyl-RAC, and aliquots of captured proteins (Bound) and unbound fraction (Supt) were analyzed by immunoblotting for BACE1, PSD95, and Flotillin 2. (D) P7 mouse brain was homogenized in a buffer containing 0.5% Lubrol WX at 4 °C for 30 min. The lysates were then subject to flotation sucrose density gradient, and an equal volume of each fraction, harvested from the top, was analyzed by immunoblotting. Fractions 4 to 6 represent the interface between 5% and 35% sucrose in the gradient and are enriched in lipid raft marker Flotillin-2. (E) Quantification of the relative distribution of BACE1 in lipid raft and nonraft fractions. **P < 0.01.

does not markedly affect prominent BACE1 localization in mossy fibers or phenocopy the loss of BACE1 expression.

To assess whether lack of S-palmitoylation affects neuronal processing of APP, brain tissue harvested at postnatal day 7 (P7) or day 60 (P60) were fractionated into a soluble protein fraction [extracted in diethylamine (DEA)] and a membrane protein fraction [extracted in radioimmunoprecipitation assay (RIPA) buffer] (8). Control immunoblots show that N-terminal and C-terminal antibodies can detect APP and its homolog APP-like protein (APLP) 2 in the input and RIPA extracts. However, the N-terminal but not the C-terminal antibodies detect the signal in the DEA extracts, indicating successful separation of soluble ectodomains from membrane-bound full-length proteins under this extraction condition (Fig. S3A). Consistent with previous findings (25), analysis of RIPA extracts revealed higher levels of BACE1 at P7 compared with P60, but no significant difference was observed between WT and 4CA mice (Fig. S3B). Immunoblot analysis revealed similar levels of ectodomains derived from APP and APLP2 in the DEA fractions of WT and 4CA brains at P7 and P60 (Fig. S3 C and D). There was a small but significant increase in the levels of soluble APLP1 in 4CA mice at P60. Consistent with an unperturbed BACE1 processing, immunoblot analysis of RIPA extracts revealed comparable levels of immature and mature APP and its homologs (Fig. S3 C and D). BACE1 cleaves APP within the ectodomain between Met^{596} and Asp^{597} (β-site) and between Tyr^{606} and Glu^{607} (β′-site) to generate +1 β–C-terminal fragment (CTF) and +11 β-CTF, respectively (1). To determine whether BACE1 S-palmitoylation introduces subtle differences in the preference of BACE1 cleavage at either site, APP CTFs were immunoprecipitated from total brain homogenates and subjected to phosphatase treatment before fractionation through Tris-Tricine gels to identify the individual CTFs (26). Immunoblot analysis using a C-terminal APP antibody revealed no difference in the relative abundance of +1 and +11 CTFs (Fig. 2 A and B) in 4CA mice. In agreement, the levels of α-CTF, generated by the processing of APP by ADAM proteases, were also unchanged in 4CA mice.

Since proteomic approaches have identified a large set of neuronal substrates for BACE1 (8), the processing of select neuronal substrates was assessed in DEA homogenates. Similar to our findings on APP and homologs, there was no quantitative difference in the levels of ectodomains of close homolog of L1 (CHL-1), contactin-2, and seizure protein 6 (SEZ6), which have been characterized as major neuronal BACE1 substrates (Fig. S3 C and D). Immunoblot analysis of RIPA extracts revealed comparable levels of immature and mature forms of these substrates, in agreement with an unperturbed BACE1 processing (Fig. S3C). Since several neuronal BACE1 substrates are thought to play an important role(s) in synapse formation and function (8, 27), we performed biochemical analysis of synaptic proteins isolated by fractionation. The analysis showed no marked difference in the abundance of presynaptic and postsynaptic proteins in fractions isolated from the brains of 4CA mice and WT littermates. The results described above provide evidence that the lack of S-palmitoylation in BACE1 does not grossly mislocalize BACE1 or result in an overt loss in its ability to enzymatically process endogenous APP as well as several neuronal substrates.

The Synaptic Activity-Dependent Release of Aβ in Vivo Is Reduced by the Lack of BACE1 S-Palmitoylation. We performed ELISA of brain homogenates of 3-mo-old WT and 4CA mice to measure the levels of endogenous Aβ peptides. The results showed no difference in the steady-state levels of Aβ40 or Aβ42 peptides (Fig. 2C). Previous studies have shown that synaptic activity dynamically modulates brain interstitial fluid (ISF) Aβ levels in vivo (28, 29). Therefore, we set out to determine whether the activity-dependent increase in ISF Aβ might be altered in 4CA mice. First, baseline ISF Aβ levels were measured in five fractions, each collected over a 3-h period. After establishing the baseline Aβ levels, 25 μM picrotoxin (PTX), a noncompetitive inhibitor of GABA$_A$ receptor, was delivered via reverse microdialysis into the hippocampus to increase neuronal activity as described (29), and the ISF Aβ in response was measured. The results showed no significant difference in baseline ISF Aβ levels in 4CA mice (Fig. 2D). As expected, there was a significant increase in Aβ levels in response to PTX treatment in WT mice (baseline 36.68 ± 2.1 vs. PTX 43.74 ± 2.25 pg/mL, $P = 0.0052$), which corresponded to an increase of 22.2 ± 8.4% over the baseline when the increase in an individual animal is compared. However, the response to PTX was blunted in 4CA mice, resulting in only a smaller nonsignificant increase (baseline 32.24 ± 2.38 vs. PTX 35.74 ± 2.95 pg/mL, $P = 0.212$), corresponding to 11.3 ± 5.8% increase (Fig. 2E). Finally, in the same samples as above, we
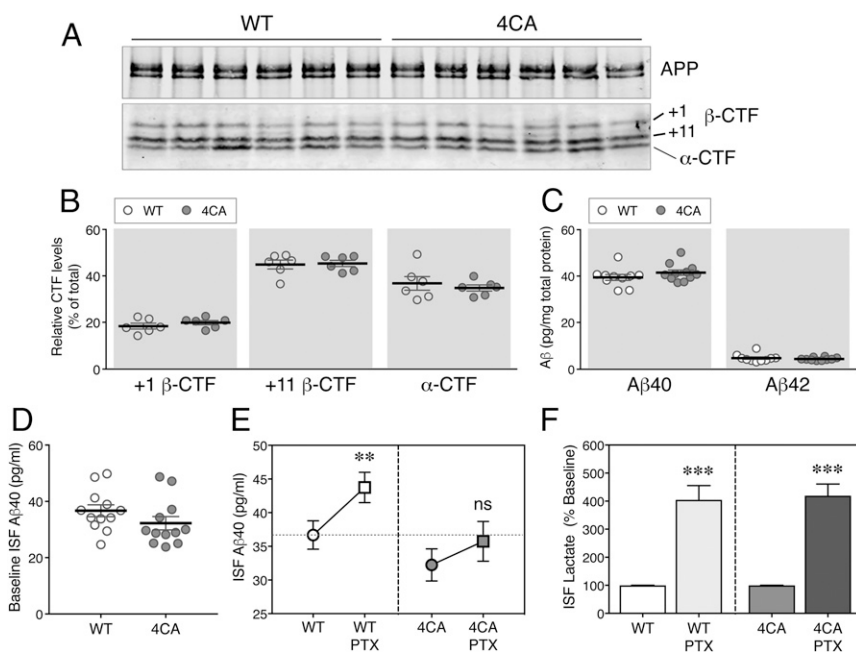

Fig. 2. The increase of ISF Aβ in response to neuronal activity is diminished in 4CA mice. (A) Full-length APP and APP CTFs in 2-mo-old WT and 4CA mouse forebrain homogenates were immunoprecipitated, subjected to dephosphorylation, and analyzed by immunoblotting. (B) The signal intensities of +1 or +11 β-CTFs and α-CTFs normalized to total APP CTFs were quantified (n = 6 WT and 6 4CA). (C) The steady-state levels of Aβ40 and Aβ42 in SDS homogenates of forebrains from 2-mo-old animals were analyzed using a V-PLEX 4G8 immunoassay (n = 10 WT and 11 4CA). (D) ISF samples were collected from 7- to 8-mo-old WT and 4CA mice (n = 12 each) by in vivo microdialysis over 15 h and analyzed by ELISA to quantify the steady-state ISF Aβ40 levels. (E) After establishing the baseline, 25 μM PTX was administered by reverse microdialysis to stimulate neuronal activity. The baseline and PTX treatment-induced Aβ40 levels were quantified and analyzed by two-way repeated measure ANOVA. ns, nonsignificant (n = 12 each). (F) The PTX-induced increase in the levels of ISF lactate, an indicator of neuronal activity, was quantified from the same samples as above. **$P < 0.01$; ***$P < 0.001$.

measured the concentrations of ISF lactate as a marker of neuronal activity (30) and found that infusion of PTX into the hippocampus significantly increased ISF lactate levels to similar magnitudes in both WT and 4CA mice (Fig. 2F). These findings suggest that the activity-dependent increase in ISF Aβ is attenuated in mice expressing S-palmitoylation–deficient BACE1.

Reduced Cerebral Amyloid Burden in the Absence of BACE1 S-Palmitoylation. Previously a high degree of correlation was reported between neuronal activity-dependent modulation of ISF Aβ and subsequent cerebral amyloid deposition in transgenic mice expressing human APP (30). To determine whether loss of BACE1 S-palmitoylation influenced the cerebral Aβ pathology, we generated 9-mo-old female PDAPP and PDAPP:4CA (PD4CA) mice. The PDAPP model overexpresses human APP harboring an APP^{V717F} familial AD-linked mutation (31). Notably, the BACE1 cleavage site is unaltered in the human transgene-derived APP. We measured Aβ levels by ELISA in hemibrains sequentially extracted in PBS (soluble forms of Aβ) and guanidine (insoluble forms of Aβ). The results showed a significant decrease in the levels of insoluble Aβ40 (0.429 ± 0.112 vs. 0.219 ± 0.017 ng/mg lysate, $P = 0.02$) and insoluble Aβ42 (1.716 ± 0.65 vs. 0.647 ± 0.063 ng/mg, $P = 0.006$) (Fig. 3A) in PD4CA compared with PDAPP mice. There were no significant differences in the levels of soluble Aβ40 (0.40 ± 0.044 vs. 0.426 ± 0.019 pg/mg, $P = 0.58$) or soluble Aβ42 (0.199 ± 0.006 vs. 0.195 ± 0.007 pg/mg, $P = 0.70$) (Fig. 3A). Next, hemibrain tissue was stained with Thioflavin S to visualize and quantify fibrillary Aβ deposits. Consistent with previous reports on Aβ deposition in the PDAPP model (31, 32), mice in both groups had developed Thioflavin S-positive Aβ deposition by 9 mo of age in the cingulate cortex and hippocampus (Fig. 3B). When the ex-

tent of deposition in the hemibrain was compared between the two groups, a significant reduction in the percent area covered with amyloid deposits was observed in PD4CA mice (0.066 ± 0.012 vs. $0.033 \pm 0.003\%$, $P = 0.02$) (Fig. 3C). In addition, noticeably fewer deposits were present in the hippocampus of PD4CA mice (Fig. 3B). Immunostaining of tissue sections with anti-Aβ+1 mAb 3D6 confirmed the reduction in percent area covered by Aβ deposits (0.708 ± 0.176 vs. $0.333 \pm 0.042\%$, $P = 0.023$) (Fig. 3C). Thus, the lack of BACE1 S-palmitoylation significantly reduced Aβ accumulation and deposition in the brains of PDAPP mice.

We extended our investigation on BACE1 S-palmitoylation using the 5XFAD line, which is a more robust model of AD amyloidosis. APP processing, cerebral amyloid levels, and amyloid deposition were analyzed in 5XFAD and 5XFAD:4CA (5X4CA mice) littermates at 4 mo of age. Analysis of full-length APP and APP CTFs by immunoprecipitation/immunoblot analysis from brain homogenates of 5XFAD and 5X4CA mice revealed no significant differences in the levels of APP CTFs (Fig. S4 A and B). ELISA analysis did not reveal a statistically significant decrease of insoluble Aβ40 (13.62 ± 1.05 vs. 10.96 ± 1.48 ng/mg lysate, $P = 0.145$) or insoluble Aβ42 (40.49 ± 2.10 vs. 36.85 ± 3.49 ng/mg, $P = 0.367$) (Fig. S4C). A z-score analysis confirmed that the levels of the insoluble Aβ in the 5X4CA cohorts were, in general, lower than the mean values of the 5XFAD cohort (Fig. S4D). Similarly, there were no significant differences in the levels of soluble Aβ40 and Aβ42 (Fig. S4C). Numerous amyloid deposits were observed by Thioflavin S staining and mAb 3D6 immunolabeling in the cortex, hippocampus, and thalamus of 5XFAD and 5X4CA mice (Fig. 3D). Quantitative analysis revealed a 35% reduction in the percentage area covered with mAb 3D6-positive amyloid deposits in 5X4CA
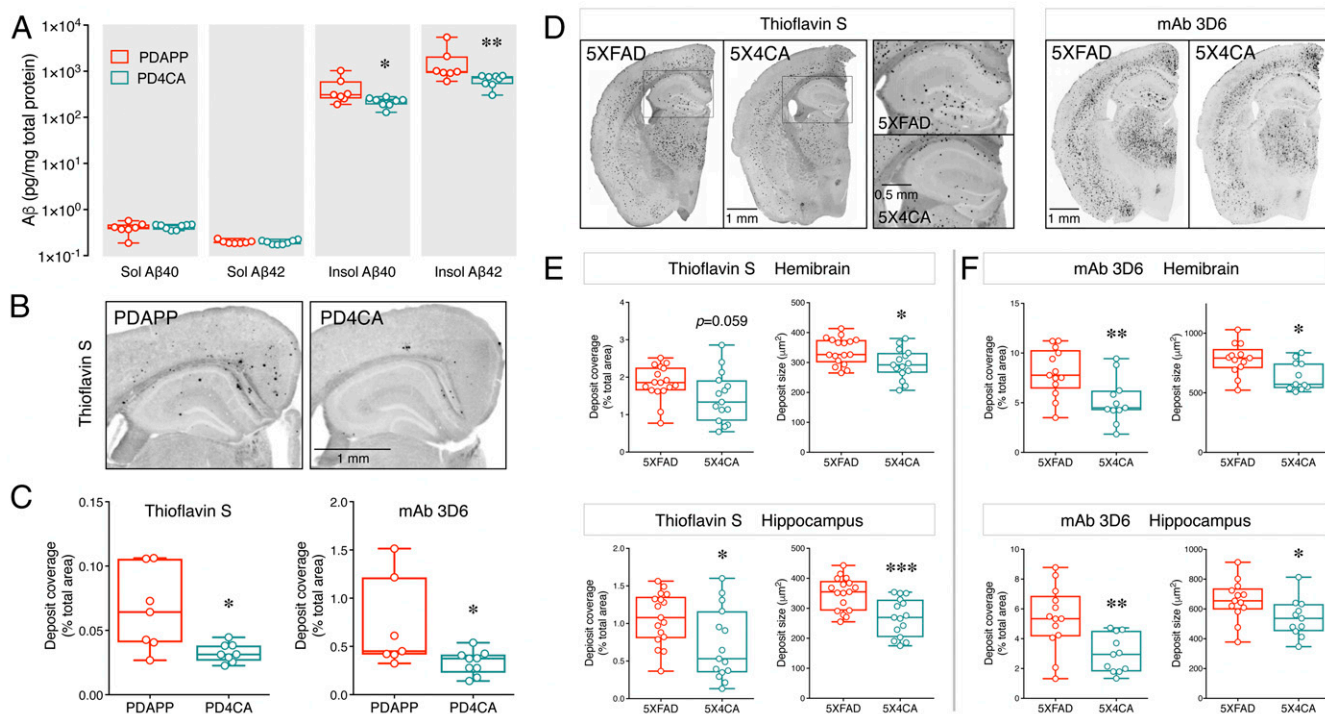

Fig. 3. Reduced amyloid deposition in AD mouse models in the absence of BACE1 S-palmitoylation. (A) Forebrain tissue harvested from 9-mo-old female PDAPP and PD4CA mice (n = 7 and 8, respectively) were sequentially homogenized in PBS and guanidine to extract soluble (Sol) and insoluble (Insol) Aβ. The levels of Aβ40 and Aβ42 in each fraction were quantified by ELISA. (B) Representative images of fibrillary Aβ deposit staining using Thioflavin S. (C) Quantification of amyloid load in hemibrain by Thioflavin S staining (n = 7 PDAPP; 8 PD4CA) and mAb 3D6 immunostaining (n = 7 PDAPP; 9 PD4CA). (D) Representative images of 4-mo-old 5XFAD and 5X4CA mice analyzed by Thioflavin S staining and mAb 3D6 immunostaining. A higher magnification of the boxed region is shown. (E and F) Quantification of amyloid load and deposit size in hemibrain and hippocampus by Thioflavin S staining (n = 17 5XFAD; 15 5X4CA) and mAb 3D6 immunostaining (n = 13 5XFAD; 11 5X4CA). *P < 0.05; **P < 0.01; ***P < 0.001.

mice ($8.05 \pm 0.66\%$ in 5XFAD vs. $5.20 \pm 0.69\%$ in 5X4CA, $P = 0.007$) (Fig. 3F). There was also a reduction in Thioflavin S-positive fibrillary Aβ deposits, but it did not reach statistical significance ($1.85 \pm 0.11\%$ vs. $1.46 \pm 0.17\%$, $P = 0.059$) (Fig. 3E). Similar to the results from PD4CA mice, fewer deposits were found in the hippocampus by mAb 3D6 staining ($5.36 \pm 0.60\%$ vs. $2.97 \pm 0.38\%$, $P = 0.004$) and Thioflavin-S staining ($1.07 \pm 0.08\%$ vs. $0.72 \pm 0.12\%$, $P = 0.021$) (Fig. 3 E and F). Taken together, the results from two transgenic mouse models demonstrate that the lack of BACE1 S-palmitoylation significantly reduces Aβ accumulation and deposition.

Reduced Dystrophic Neurite Accumulation of S-Palmitoylation–Deficient BACE1. In analyzing the amyloid deposition data, we noticed a significant decrease in the average fibrillar amyloid deposit size in 5X4CA mice as visualized by Thioflavin S staining of the hemibrain (339 ± 10.86 vs. 294.3 ± 12.95 μm^2, $P = 0.012$) or selectively in the hippocampus (348.3 ± 13.37 vs. 269.6 ± 16.36 μm^2, $P = 0.0007$) (Fig. 3E). The mean amyloid deposit size as observed by mAb 3D6 immunostaining was twice as large compared with Thioflavin S staining, but, still, the deposit size was significantly smaller in 5X4CA than 5XFAD mice (hemibrain, 781.6 ± 36.84 vs. 640.3 ± 36.41 μm^2, $P = 0.012$; hippocampus, 657.2 ± 37.84 vs. 540.2 ± 38.7 μm^2, $P = 0.428$) (Fig. 3F). As BACE1 has previously been shown to accumulate in dystrophic neurites in close proximity to amyloid deposits along with APP, contributing to local amyloid production and deposition (33–35), we determined the relative accumulation of BACE1 at peri-deposit regions in 5XFAD and 5X4CA mice (Fig. 4A). Quantitative analysis revealed that 5X4CA mice had increased frequency of deposits with lower levels of BACE1 in dystrophic neurites relative to mAb 3D6 signal intensity in individual deposit sites in the cortex and hippocampus (Fig. 4B) ($P < 0.0001$ by Kolmogorov–Smirnov test of cumulative frequency distribution analysis). The mean ratio of BACE1:3D6 signal intensity (0.2503 ± 0.005 vs. 0.2098 ± 0.006, $P < 0.0001$), as well as integrated intensity ($3.71 \pm 0.12 \times 10^5$ vs. 3.00 vs. 0.11×10^5, $P < 0.0001$), was also significantly lower in 5X4CA mice in comparison with 5XFAD mice (Fig. 4C), indicating less BACE1 accumulation in dystrophic neurites, and thus lower presynaptic Aβ production near the sites of amyloid deposition. Finally, we immunostained tissue sections for LAMP1 as a marker to visualize dystrophic neurites (36). There was no significant difference in LAMP1 accumulation in 5XFAD and 5X4CA mice at peri-deposit sites (Fig. 4 D and E), indicating a specific reduction of BACE1 in 5X4CA mice in dystrophic neurites independent of the accumulation of other neuronal proteins.

S-Palmitoylation Is Required for BACE1 Localization in Neuron-Specific Compartments. Next, we sought to investigate whether the observed differences in BACE1 accumulation in dystrophic neurites is due to differences in intrinsic S-palmitoylation–dependent neuronal trafficking of BACE1. Since the currently available antibodies are not suitable to label endogenous BACE1 in dendrites and dendritic spines of neurons in the brain, we pursued this line of investigation using YFP-tagged BACE1 expressed in cultured neurons, as previously described (22, 37). Cultured hippocampal neurons were cotransfected at 11 d in vitro (DIV11) with constructs expressing wt BACE1-YFP (wt-YFP) or 4CA-BACE1-YFP (4CA-YFP) and low levels of mApple-Actin (to visualize spines), and cultured to DIV15, a stage at which spines are abundant. The first bifurcation of the apical dendrite was imaged to assess BACE1 localization in spines. As expected, wt-YFP was present along the dendrites and clearly overlapped with actin-enriched spines (Fig. 5A). Remarkably, 4CA-YFP was conspicuously absent from the vast majority of the spines, restricted instead to the shaft of the dendrites (Fig. 5A). The expression of 4CA-YFP did not alter the density of actin-positive spines in the transfected neurons. The percentage of actin-positive spines containing
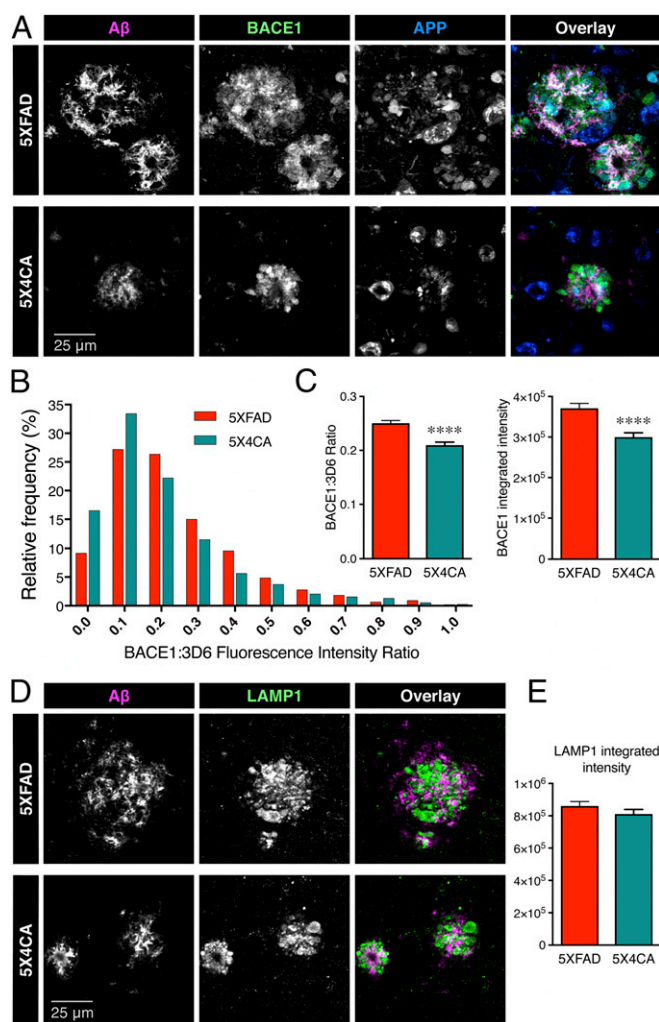
Fig. 4. Reduced accumulation of BACE1 in dystrophic neurites in the absence of BACE1 S-palmitoylation. (A) Representative images of immunofluorescence labeling of Aβ deposits (mAb 3D6, magenta), APP (blue), and BACE1 (green). (B) Frequency distribution analysis of BACE1 fluorescence intensity relative to that of Aβ in individual amyloid deposits. All nonoverlapping deposits were counted within equal areas of four cortical regions and the hippocampus (n = 5XFAD 1,782 deposits from four mice; 5X4CA 1,443 deposits from four mice). (C) The graphs represent the mean ratio of BACE1 to Aβ fluorescence intensity and the mean integrated intensity of BACE1 immunostaining. (D) Representative images of immunofluorescence labeling of Aβ deposits (mAb 3D6, magenta) and LAMP1 (green). (E) Integrated intensity of LAMP1 staining in nonoverlapping deposits in four cortical regions and the hippocampus (n = 5XFAD 1,417 deposits from four mice; 5X4CA 915 deposits from four mice). ****$P < 0.0001$.

BACE1 along defined lengths of dendrites was quantified. Whereas wt-YFP was present in ~72% of the spines, 4CA-YFP was present in only ~25% of actin-positive spines ($P < 0.0001$; n = 23 wt- and 24 4CA-YFP expressing neurons) (Fig. 5B). Thus, palmitoylation-deficient BACE1 was significantly impaired in dendritic spine localization in mature hippocampal neurons.

In the small fraction of spines that were counted as positive for 4CA-YFP, the fluorescence intensity was still lower than that of wt-YFP intensity. To exclude the possibility that 4CA-YFP levels were in general low throughout the entire neuron with no specific change in spine localization per se, we assessed BACE1 spine localization in greater detail. The relative fluorescence signal in the spine head vs. the base of each mushroom-type and stubby-type spine was quantified using the actin signal as a reference for the spine area (Fig.
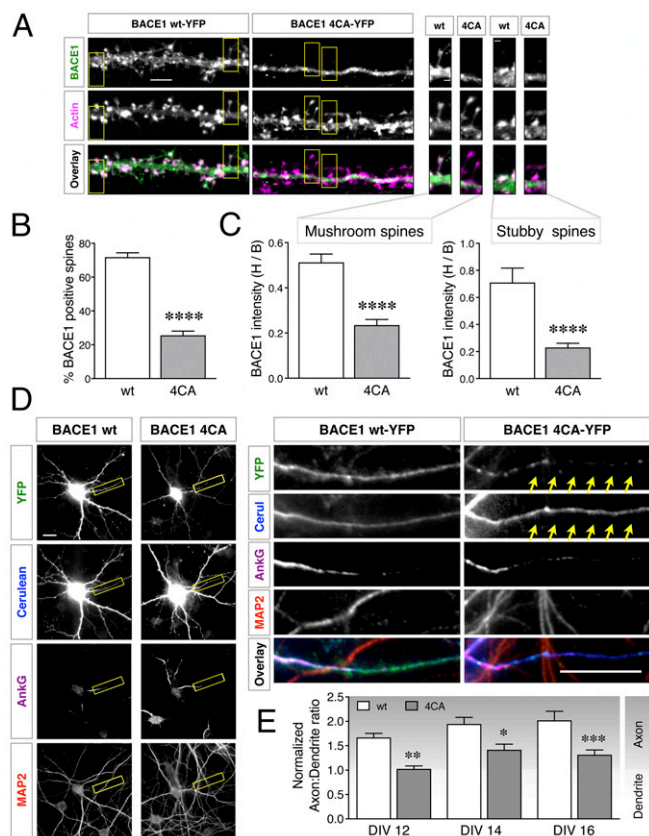
Fig. 5. Modulation of BACE1 trafficking in neurons by S-palmitoylation. (*A*) Hippocampal neurons were cotransfected with mApple-Actin and either YFP-tagged BACE1 wt or 4CA constructs. Neurons were fixed 4 d later (DIV15) and analyzed by microscopy. A higher magnification of the boxed regions depicting mushroom or stubby spines are shown on the *Right*. (Scale bars: *Left*, 5 μm; *Right*, 1 μm.) (*B*) Quantification of the percentage of actin-positive spines that contain BACE1 (*n* = 23 WT and 24 4CA neurons from three independent cultures). (*C*) Quantification of BACE1 intensity in spine head relative to the base of the spine (H/B) (*n* = WT 279 and 4CA 300 mushroom spines; WT 61 and 4CA 67 stubby spines). (*D*) Neurons coexpressing Cerulean and BACE1-YFP were fixed at DIV16 and immunostained for AnkG and MAP2, to identify the axon initial segment and dendrites, respectively. A higher magnification of the boxed region is shown on the *Right*. The arrows highlight the axon. (Scale bars, 20 μm.) (*E*) Neurons were transfected on DIV10, and nADRs were calculated on DIV12 (*n* = 30 neurons each), DIV14 (*n* = 30 neurons each), or DIV16 (*n* = WT 34 and 4CA 35 neurons). Results are from at least three independent cultures, each analyzed in parallel on all time points. *$P < 0.05$; **$P < 0.01$; ***$P < 0.001$; ****$P < 0.0001$.

5*A*). This analysis revealed a clear, significant decrease of the head/base ratio of 4CA-YFP in spines of both types ($P < 0.0001$; *n* = 22 wt and 19 4CA) (Fig. 5*C*). These data show that, while 4CA-BACE1 is able to localize to the dendrite shaft, it is either not transported into, or retained at, the spines as efficiently as wt BACE1, suggesting that S-palmitoylation is necessary for this neuron-specific targeting of BACE1 to dendritic spines.

BACE1 undergoes polarized sorting in vivo and in transfected hippocampal neurons (22, 37). BACE1 targeting to axons involves a transcytotic mechanism whereby BACE1 is internalized from dendrites and trafficked in an exclusively retrograde direction to the soma and subsequently routed to the axon in a Rab11-dependent manner (22, 37, 38). Therefore, axonal localization of BACE1 was quantified to assess whether there is a deficiency in axonal targeting of 4CA-YFP. In this experiment, BACE1-YFP and Cerulean were expressed from a single plasmid to ensure comparable expression of the two fluorescent proteins, and the axon:dendrite ratio of randomly distributed Cerulean was used to calculate a normalized

axon:dendrite ratio (nADR) for BACE1 (22, 39) (Fig. 5*D*). The nADR for wt-YFP in mature neurons progressively increased from 1.7 to 2 when analyzed at DIV12, -14, and -16, indicating preferential localization in axons in mature neurons (Fig. 5*E*). However, the nADR for 4CA-YFP was significantly lower than that of wt-YFP, ranging between 1 and 1.4 (Fig. 5*E*). Thus, S-palmitoylation is required for axonal BACE1 enrichment in cultured hippocampal neurons.

The Lack of BACE1 S-Palmitoylation Mitigates Memory Deficits in 5XFAD Mice. Cognitive dysfunction is a characteristic feature in several transgenic mouse models of amyloidosis (40). Aβ pathology-dependent memory deficits in the 5XFAD model have been characterized using the Y-maze and fear conditioning tests (41, 42). We performed these memory tests to determine whether the differences in cerebral amyloid burden in 5XFAD mice lacking BACE1 S-palmitoylation can attenuate memory deficits in this model. First, the Y-maze test was performed to assess hippocampus-dependent spatial working memory. No significant difference was observed between WT and 4CA mice in the number of arm entries or spontaneous alternations in the Y-maze (Fig. 6*A*). As expected (42), 5XFAD mice showed a significant decrease in the percentage of spontaneous alternation. Interestingly, 5X4CA mice showed a significantly higher percentage of alternation compared with 5XFAD mice (Fig. 6*A*).
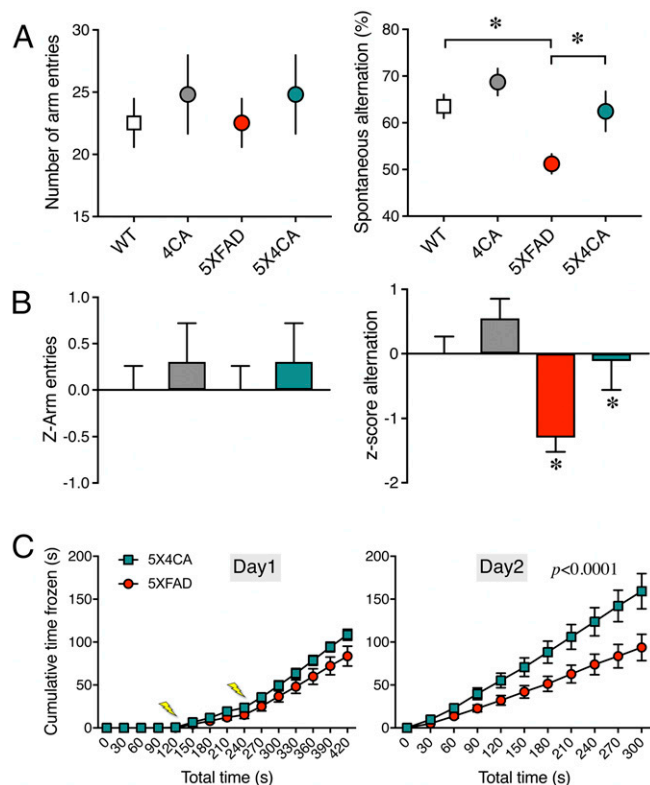

Fig. 6. The lack of BACE1 S-palmitoylation mitigates cognitive deficits in 5XFAD mice. (*A*) Cohorts of mice of the indicated genotypes were assessed for spatial working memory in the Y-maze test. The number of arm entries and the spontaneous alternation behavior were quantified (*n* = WT 14; 4CA 12; 5XFAD 15; 5X4CA 11 mice). (*B*) The normalized z-scores of the test results were calculated to assess the significance of the differences observed in the different cohorts of mice. (*C*) Hippocampal-dependent associative learning and memory task. 5XFAD and 5X4CA animals were exposed to the contextual fear conditioning paradigm, and freezing behavior was measured either during the training (day 1) or 24 h after the conditioning (day 2) (*n* = 5XFAD 19; 5X4CA 12 mice). The lightning bolts indicate the time when the electric shocks were delivered. *$P < 0.05$.

The number of arm entries recorded for 5XFAD and 5X4CA animals was comparable, indicating that the observed change in the percentage alternation is not due to differences in their motor activity. To test the significance of the differences observed in the different cohorts, we performed z-normalization as described (43, 44). The normalized z-score confirmed a significant impairment in the 5XFAD cohort compared with the WT and a significant rescue of the impairment in the 5X4CA cohort (Fig. 6B). Second, the contextual fear conditioning test was performed on 5XFAD and 5X4CA mice to assess hippocampus-dependent associative learning. For the acquisition of contextual fear conditioning, the animals were placed in the conditioning context and exposed to two brief foot shocks with a 2-min interval. There was no difference between 5XFAD and 5X4CA mice in their locomotor response to the testing chamber. Moreover, the mice in both groups responded to the successive foot shocks with very low levels of movement, indicating the acquisition of fear conditioning (Fig. 6C). On the following day, when the animals were tested for the contextual memory in the absence of foot shocks, the 5X4CA mice showed significantly greater immobility compared with 5XFAD mice (Fig. 6C). Taken together, these data indicate that reduced amyloid burden due to the lack of BACE1 S-palmitoylation ameliorates behavior deficits in spatial working memory and associative learning in 5XFAD mice.

Discussion

In this study, we assessed the significance of BACE1 S-palmitoylation as a modulator of Aβ-related AD pathology by generating 4CA knock-in mice and crossing them to mouse models of amyloidosis. The lack of S-palmitoylation reduces raft association of BACE1 but does not affect its steady-state levels or proteolysis of APP and, importantly, several neuronal substrates with roles in synaptic plasticity and neurite outgrowth (21, 27, 45). Indeed, the inability of direct BACE1 inhibition to spare essential neuronal substrates is a key issue given the reported abnormalities in memory and spine density in BACE1 KO mice (45). In cultured hippocampal neurons, S-palmitoylation is required for efficient BACE1 targeting to dendritic spines and transport to axons. Remarkably, mice expressing 4CA BACE1 show significant impairment in synaptic activity-induced Aβ production and lower cerebral amyloid burden in PDAPP and 5XFAD transgenic backgrounds. Moreover, the behavioral deficits in the 5XFAD model, which exhibits a more rapid onset of pathogenesis, are mitigated by the expression of BACE1 lacking S-palmitoylation. These findings highlight the physiological role of BACE1 S-palmitoylation as a modulator of amyloid burden and its effects in vivo.

S-palmitoylation on juxtamembrane cysteines is thought to affect the conformation of transmembrane proteins (46), as in the case of LRP6, where palmitoylation-mediated tilting of the transmembrane domain is required for efficient endoplasmic reticulum exit of nascent LRP6 (47). In the case of BACE1, our in vivo studies do not support an overt effect of S-palmitoylation on BACE1 steady-state accumulation. A substantial amount of BACE1 in the brain was modified by S-palmitoylation, as revealed by acyl-RAC assays and the significant reduction in raft distribution of BACE1 in 4CA mice. However, BACE1 processing of multiple substrates in the brain was indistinguishable between WT and 4CA mice. Thus, the lack of palmitoylation does not affect BACE1 biogenesis or its enzymatic activity. This observation is consistent with a lack of difference in Aβ generation in cultured cell lines and in neurons overexpressing wt or 4CA mutant BACE1 (10, 17). Nevertheless, our in vivo studies in the 4CA knock-in model, which ensures accurate spatial and temporal regulation of mutant BACE1 expression at physiological levels without the presence of endogenous wt BACE1, reveal that S-palmitoylation of BACE1 enables its efficient targeting to specific neuronal compartments and is also critical for elevated Aβ production in vivo in response to synaptic activation.

As BACE1 is an essential enzyme that initiates amyloidogenic processing of APP, several examples in the literature exemplify how manipulations that modify BACE1 levels or perturbation of cellular mechanisms responsible for BACE1 trafficking result in the modulation of APP processing and Aβ production in cultured cells (9). We generated a knock-in model to enable functional analysis of S-palmitoylation–deficient BACE1 at physiological expression levels in vivo and gain insights on AD pathogenesis. Our results reveal that S-palmitoylation of BACE1 regulates synaptic activity-driven Aβ production and significantly contributes to amyloid deposition in the brain. Aside from the characterization of BACE1 knockout mice crossed with AD mouse models where there is an obvious diminution of Aβ generation (9), only a few studies have reported a significant influence of cerebral amyloid burden following genetic manipulations that affect BACE1 levels and/or localization in vivo. Notably, whereas the loss of GGA3 expression significantly increases BACE1 levels and enzyme activity in vitro and in vivo, increased Aβ production was not observed in vivo (48). In a recent study, the loss of the dynein motor adaptor snapin was found to cause presynaptic BACE1 accumulation and an increase in Aβ production in the brain. Moreover, adeno-associated viral overexpression of snapin decreased presynaptic BACE1 and attenuated Aβ production and deposition (49). In another study, high-level expression of transgenic BACE1 increased BACE1 processing of APP in the soma but led to a significant reduction in Aβ deposits (50). Our findings and the data detailed in these reports highlight the significance of presynaptic BACE1 processing of APP for the development of amyloid pathology in the brain and are consistent with compelling evidence that APP is trafficked anterogradely along peripheral and central axons and proteolytically processed during transit (26, 51).

It is well established that S-palmitoylation is a critical modification of integral and peripheral membrane neuronal proteins. Notably, the dynamic synaptic localization of polytopic ionotropic glutamate receptors and many of their binding partners that lack a transmembrane domain (such as PSD-95 and GRIP2b) are regulated by palmitoylation (13–16, 52, 53). Juxtamembrane palmitoylation also contributes to dendritic spine localization of synapse differentiation-inducing gene protein 1, a type II transmembrane protein (54). Our results show that S-palmitoylation of the type I transmembrane protein BACE1 is critical for efficient localization in dendritic spines in cultured hippocampal neurons. Interestingly, axonal targeting of BACE1 also appears to be influenced by S-palmitoylation. Consistent with our previous report, the higher nADR for wt BACE1 is due to a progressive enrichment of BACE1 in the axon as the neurons matured in culture; 4CA-BACE1 fails to be enriched to the same degree, suggesting that S-palmitoylation is required for steady-state axonal enrichment of BACE1 in mature neurons. This later finding is in accordance with S-palmitoylation playing an essential role in mediating axonal targeting of membrane-tethered cytosolic proteins GAP-43, paralemmin, and GAD65 (55, 56). S-palmitoylation has also been recognized as the signal that directs sorting of GRIP1b and AKAP 79/150 to recycling endosomes in dendrites and GAD65 to axon-specific endosomes (56–58). Taken together with our previous characterization of dendrite-to-axon transcytosis of BACE1, mediated by EHD1/3 and Rab11-dependent endocytic sorting (22, 37, 38), the remarkable differences in dendritic spine localization and axonal targeting of wt and 4CA-BACE1 in cultured hippocampal neurons suggest a potential mechanistic link between S-palmitoylation and polarized sorting of BACE1 in endosomes.

The 4CA genetic background had a significant effect in lowering insoluble Aβ40 and Aβ42 levels in PDAPP mice, but not in 5XFAD mice. This apparent discrepancy is not unexpected because of a key difference in the transgene-derived human APP expressed in these two AD models. Whereas the human APP expressed in the PDAPP model has the wt residues K670/ M671 immediately preceding the primary BACE1 cleavage site in APP, the APP expressed in the 5XFAD model harbors the familial

AD-linked "Swedish" double mutation K670N/M671L (31, 42). It has been long recognized that BACE1 processing of wt APP occurs mainly during endocytic transit but BACE1 cleavage of APP$^{K670N/M671L}$ can occur during secretory trafficking, as early as the medial Golgi compartment (59, 60). Consequently, our results could mean that the lack of S-palmitoylation has a significant effect in lowering Aβ levels in vivo by modulating BACE1 cleavage of APP in endosomes. Compelling evidence exists for the contribution of activity-dependent Aβ production to cerebral amyloid burden (30, 61). The finding that activity-induced increase of Aβ, but not steady-state ISF Aβ, was significantly lower in 4CA mice also provides additional insights into the mechanisms that influence Aβ production in this context. Since endocytosis mechanisms account for the vast majority of synaptic activity-induced ISF Aβ (29), the observed differences raise the possibility that activity-dependent mechanisms might regulate BACE1 S-palmitoylation and localization in endosomes in a manner that promotes amyloidogenic APP processing.

Despite the lack of a significant effect of BACE1 S-palmitoylation on APP processing or insoluble Aβ levels in 5XFAD mice, the cerebral amyloid burden was significantly lowered in both PDAPP and 5XFAD models in the 4CA background. The cerebral amyloid burden is the result of complex dynamics between Aβ production and release, extracellular proteolysis, aggregation/fibril formation, deposition, and clearance. Thus, a plausible explanation for these results is that, in addition to Aβ production, other neuronal mechanisms are responsible for the accrual of Aβ in deposits. For example, our results show that S-palmitoylation–deficient BACE1 fails to undergo enrichment in the axonal compartment in cultured neurons and accumulates to a lesser extent in dystrophic neurites near amyloid deposits in the brain. Since BACE1 accumulation in dystrophic axon terminals is thought to significantly contribute to amyloid deposition through a positive feedback of local Aβ production (33, 34, 62), 4CA mice might be lacking a significant proportion of this presynaptic Aβ component. Furthermore, the subcellular location of Aβ production (perikaryal versus axonal APP proteolysis) and regional differences in neuronal activity markedly influence amyloid deposition independent of the extent to which APP undergoes amyloidogenic processing (30, 50). It would be interesting to examine the selective contribution of BACE1 S-palmitoylation to regional Aβ production and deposition. The contribution of BACE1 S-palmitoylation to hippocampal Aβ deposition is notable and functionally significant as evidenced by the mitigation of cognitive deficits in 5X4CA mice: enhanced working memory observed in the spontaneous Y-maze alternation test and improved retention of contextual memory observed as increased freezing to the context in the fear conditioning test. These behavioral results are consistent with previous studies showing improvement of AD mouse models in memory tasks after experimental manipulations that reduced the cerebral amyloid burden (41). Although the mechanisms regulating BACE1 S-palmitoylation remain to be determined, we previously reported that subunits of the γ-secretase complex also undergo S-palmitoylation (63) and that ablation of this modification reduced cerebral amyloid burden in vivo (64), implicating a potential mechanistic link between these proteases and their lipid association that warrants further investigation. Future characterization of the enzymes and mechanisms involved in the dynamics of BACE1 S-palmitoylation/depalmitoylation in the brain might potentially advance novel avenues to manipulate Aβ levels and mitigate cognitive decline for disease modification.

Materials and Methods

Mice. BACE1 4CA mice were generated by genOway and were maintained in-house. A targeting vector was constructed with two DNA fragments corresponding to the short and long arms PCR amplified from C57BL/6 genomic DNA. The sequence was modified by inserting a Neo selection cassette with flanking loxP sites 150 bp upstream of exon 9 and point mutations (Cys/Ala

substitutions) at the codons corresponding to the four S-palmitoylated residues in exon 9. A Diptheria Toxin A cassette was placed at the extremity of the long arm to aid in negative selection. Successful homologous recombination in C57BL/6 mouse embryonic stem cells was identified by PCR screening and sequencing of the region containing the point mutations and was validated by Southern blot analysis using the 5′ external probe and an internal 3′ probe within the Neo cassette. Targeted ES cells were injected into C57BL/6 blastocysts to generate chimeras. Highly chimeric males were mated with C57BL/6 Cre deleter females to achieve germline transmission and the generation of Neo-excised heterozygous knock-in mice. Homozygous 4CA animals were generated at the expected frequency by intercrossing heterozygous animals. 4CA animals were maintained in the C57BL/6 background and bred to 5XFAD animals (C57BL/6/SJL mixed background) and PDAPP animals (C57BL/6 background). All procedures related to animal care and treatment conformed to the policies of the Institutional Animal Care and Use Committee at the University of Chicago.

Antibodies. The following primary antibodies were used: BACE1 antibodies, rabbit mAb BACE1 (EPR3956; GeneTex) and anti-BACE1 human IgG (kindly provided by Jasvinder Atwal, Genentech, South San Francisco, CA); APP antibodies, NTH452 [a rabbit polyclonal antibody (pAb) generated against a fusion protein corresponding to APP ectodomain residues 45 to 265 and C-terminal pAb CTM1] (63); APLP2 antibodies, ectodomain pAb D2II (65) and C-terminal pAb CT12 (66); APLP1 antibodies, A1NT (a rabbit pAb generated against a fusion protein corresponding to mouse APLP1 ectodomain residues 293 to 583 and C-terminal pAb CT11) (67); Aβ antibodies, mAb 3D6 (kindly provided by Dale Schenk, Elan Corporation PLC, South San Francisco, CA) and mAbs HJ2 (anti–Aβ35-40), HJ7.4, and mAb HJ5.1 (anti–Aβ37-42), which have been described (30); pAb CHL-1 and contactin-2 (R&D Systems); pAb SEZ6 (kindly provided by Jenny Gunnersen, The University of Melbourne, Melbourne, Australia); mAb PSD-95 and mAb AnkyrinG (clones K28/43 and N106/36, respectively; the University of California, Davis/NIH NeuroMab Facility); pAb Flotillin-2 (64); pAb MAP2 (Millipore); mAb phospho-Neurofilament H (SMI 31; BioLegend); mAb LAMP1 (clone 1D4B, Developmental Studies Hybridoma Bank); and actin mAb (Proteintech). Alexa Fluor-conjugated secondary antibodies were purchased from Molecular Probes.

Immunoblot Analysis. Detergent lysates of mouse brain tissue were prepared as described previously (68). Lipid raft fractionation analysis of Lubrol WX extracts of mouse brain tissue by discontinuous flotation density gradients was performed as described (20). For separating soluble and membrane proteins, the brains were homogenized as described (8) in 10 volumes (wt/vol) of 0.2% diethylamine (DEA) containing 50 mM NaCl (pH 10) and protease inhibitors and clarified by ultracentrifugation at $100,000 \times g$ for 30 min. The supernatant was neutralized by the addition of 10% 0.5 M Tris·HCl, pH 6.8, and saved as the DEA-soluble fraction. The pellet was homogenized with RIPA buffer and then cleared by ultracentrifugation for 30 min at $100,000 \times g$ to obtain the RIPA-soluble fraction. For the analysis of mouse APP CTFs, forebrain homogenates were immunoprecipitated using pAb CTM1 and treated with bacteriophage λ protein phosphatase (New England Biolabs) as described (26). The samples were resolved by SDS/PAGE on Tris-Tricine gels and analyzed by immunoblotting. The primary antibodies used to probe Western blots are listed above. The blots were developed with IR800 anti-rabbit and IR680 anti-mouse secondary antibodies, and the signal intensities were quantified using the Odyssey Infrared Imaging System (LI-COR Biosciences).

Detection of BACE1 Palmitoylation by Acyl-RAC. Protein palmitoylation was detected in mouse brain lysate using a modified Acyl-RAC assay (19). Briefly, crude membrane proteins isolated from mouse brain were incubated in blocking buffer (100 mM Hepes, 1 mM EDTA, 2.5% SDS, 10 mM N-ethyl maleimide, 1 mM PMSF, and protease inhibitors) at 40 °C for 10 min with frequent vortexing to block free cysteine residues on proteins. The blocking reagent was removed by methanol/chloroform precipitation and proteins were resuspended in binding buffer (100 mM Hepes, 1 mM EDTA, 1% SDS, pH 7.5, 1 mM PMSF and protease inhibitors). Half of the sample was treated with 2 M NH₂OH to remove acyl groups from cysteine residues while the other half was treated with 2 M NaCl as a negative control. The samples were then incubated with thiopropyl Sepharose (Sigma) beads for 3 h at room temperature to pull down proteins via the newly liberated cysteines. Beads were washed five times with binding buffer and eluted in binding buffer containing 50 mM DTT. Aliquots of the samples were analyzed by SDS/PAGE and Western blot analysis using the indicated antibodies.

Histology and Immunohistochemistry. Hemibrains were processed as described, serially cut into 40-μm-thick coronal sections, and immunostained using mAb 3D6 following a free-floating procedure (69). To stain fibrillar amyloid deposits,

brain sections were stained with 0.5% Thioflavin S (Sigma) in 50% ethanol for 15 min and sequentially washed with 50% ethanol and PBS before mounting. Stained sections were imaged on a CRi Panoramic Scan Whole Slide Scanner (Cambridge Research and Instrumentation) using a 40× (0.95 N.A.) long working distance Zeiss objective and Allied Vision Technologies Stingray F146C, 4.6-μm pixel size color camera. Tiled images were analyzed using 3DHistech software (Cambridge Research and Instrumentation). Wide-field epifluorescence images were acquired using a Nikon TE2000 microscope with 10× (N.A. 0.3) and 20× (N.A. 0.75) objectives. Confocal images were acquired on a Leica SP5 II STED-CW Superresolution laser scanning confocal microscope with 20× (N.A. 0.8) and 40× (N.A. 0.8) objectives. Images were processed using ImageJ software (70).

Image Analysis. For the quantification of ThioflavinS and mAb 3D6 staining, five to eight sections per mouse were analyzed. Tiled images were thresholded to define amyloid deposits over background fluorescence, and the pixel area relative to the total area of interest (hippocampus or hemibrain) was quantified using ImageJ (70). Similarly, peri-deposit BACE1 fluorescence intensity was quantified from cortical and hippocampal regions from four animals per group (with cerebral amyloid burden closest to the mean of the group). The mAb 3D6 and BACE1 images were thresholded to generate a combined binary mask for each image, and deposit regions were defined using integrated morphometry analysis tools using MetaMorph 7.5 software (Molecular Dynamics). Integrated intensity data for BACE1 and mAb 3D6 were measured for well-defined deposit regions to obtain the BACE1 to 3D6 ratio for individual deposits.

Aβ ELISA. For endogenous Aβ ELISA, brains of 3-mo-old WT and 4CA mouse brains were homogenized, in 10 volumes (wt/vol) of 1% SDS in PBS and protease inhibitors, and clarified by centrifugation. Aβ40 and Aβ42 levels were measured using a V-PLEX Plus Aβ Peptide Panel 1 (4G8) Kit (Meso Scale Discovery). For transgenic Aβ ELISA, hemibrains of 4- (5XFAD) or 9-mo-old (PDAPP) female transgenic mice were sequentially extracted in 5 volumes (wt/vol) of PBS and 5 M guanidine in the presence of protease inhibitors. Human Aβ40 and Aβ42 in the PBS and guanidine soluble fractions were measured by ELISA using mAb HJ2 and HJ7.4 for the capture and biotinylated mAb HJ5.1 for the detection as described (30).

In Vivo Microdialysis. WT and 4CA animals of both sexes at 7 to 8 mo of age underwent stereotactic surgery to implant guide cannulas (BR-style Bioanalytical Systems) into the left hippocampus (from bregma: anteroposterior (AP), −3.1 mm; mediolateral (M/L), −2.5 mm; dorsoventral (D/V), −1.2 mm at 12° angle), which were secured with dental cement. One day after the mice were acclimated to Raturn sampling cages (Bioanalytical Systems), microdialysis probes (2 mm; 39 kDa molecular mass cutoff, BR-style; Bioanalytical Systems) were inserted into the guide cannula and connected to a syringe pump. Artificial CSF (aCSF) (1.3 mM CaCl$_2$, 1.2 mM MgSO$_4$, 3 mM KCl, 0.4 mM KH$_2$PO$_4$, 25 mM NaHCO$_3$, 122 mM NaCl, 0.15% BSA; pH 7.35) was infused at 1 μL/min, and ISF was collected at 1 μL/min into 3-h fractions. The next day, after five fractions (15 h) of baseline ISF collection, PTX was delivered at 25 μM in aCSF via reverse microdialysis as previously described (29, 30) to increase neuronal activity for 3 h. At the end of the experiment, the left hemisphere was collected after perfusion, and Cresyl Violet staining was used to confirm probe placement. Murine Aβ40 in the ISF fractions described above was measured by ELISA using mAb HJ2 for the capture and mAb JHJ5.1 for the detection (30). ISF lactate was measured in the same microdialysis fractions using a YSI 2900 Analyzer according to the manufacturer's instructions.

Behavioral Analysis. Mice were tested for spontaneous alternation on a Y-maze as they freely explored through the maze during an 8-min session. The sequence and the total number of arm entries (when all four limbs are within the arm) were recorded. An alternation is defined as entries into all three arms on consecutive occasions. Therefore, the number of maximum alternations equals the total number of arm entries minus two. The percentage of alternations was calculated as (the number of triads containing entries into all three arms/maximum alternations) × 100 and analyzed by ANOVA. For contextual fear conditioning, each animal was trained by placing it in a conditioning chamber (ActiMetrics) and allowing it to explore. After a 2-min habituation period, a brief, mild foot shock (1.0 mA, 2 s) was delivered through a grid floor at the bottom of the cage by a Coulbourn Instrument shocker. After an interval of

2 min, the animal was presented again with the foot shock to strengthen the association. The animal remained in the chamber for an additional 3 min before being returned to its home cage. On the following day, the animal was returned to the same conditioning chamber, and its movements were recorded for 5 min. Mice were monitored using a video-based system (FreezeFrame 4 software; ActiMetrics) at the rate of 4 Hz, to automatically monitor baseline motor activity with a sensitivity to detect movements as small as 1 mm. Freezing was defined as the absence of all movement except that required for respiration; in our experiments, a minimum 1-s bout of immobility was scored as freezing. The cumulative time frozen during acquisition and retention of contextual fear conditioning was compared between the two groups using two-way ANOVA (Prism 7).

Primary Hippocampal Neuron Culture and the Analysis of BACE1 Localization. Primary hippocampal neuron cultures were generated from embryonic day 17 to 18 rat hippocampi, plated on poly-D-lysine–coated coverslips, and maintained in Neurobasal supplemented with serum-free B27 and 2 mM GlutaMAX (Invitrogen). For dendritic localization analysis, neurons were cotransfected on DIV11 using Lipofectamine 2000 with cDNA constructs encoding mApple-actin and either BACE1 wt-YFP or BACE 4CA-YFP. Neurons were fixed on DIV15, and confocal images of the apical dendrite in the area of the first bifurcation were acquired using a Leica SP5 Tandem Scanner Spectral 2-Photon confocal microscope with a 100× objective (N.A. 1.46). All image processing was performed using ImageJ (70) and MetaMorph image analysis software (Molecular Devices). Dendritic spines were identified by enriched mApple-actin signal dotted along the dendrite and were separated into two morphologically distinct categories: "mushroom" and "stubby" spines. Manual quantifications of BACE1 spine localization were performed using the cell counter plugin in ImageJ. BACE1-YFP fluorescence intensity in spine head and base was performed using MetaMorph. After subtracting background fluorescence using statistical correction, regions were manually created around the spine head and at the base of the dendrite immediately below the spine head using the mApple-actin fluorescence as the reference. The regions of interest were then transferred to the YFP image, and the integrated intensity was measured. The fluorescence intensity at the head and base of each dendritic spine was used to calculate the head/base ratio.

For axon:dendrite ratio (ADR) analysis, neurons were transfected at DIV11 with a plasmid that coexpresses BACE1 (wt-YFP or 4CA-YFP) and Cerulean. Transfected neurons were then fixed 1, 3, or 5 d after transfection, and dendrites and the axon initial segment were labeled by staining with anti-MAP2 and anti-AnkG antibodies, respectively. Wide-field epifluorescence images were acquired using a Nikon TE2000 microscope with a 60× objective (N.A. 1.49). Briefly, the average YFP and Cerulean fluorescence intensities were measured along 100- to 200-μm-long 1-pixel-wide line segments traced on three representative sections of dendrites and in the proximity of the initial axon segment in each neuron. Normalized ADRs were then calculated by dividing the raw ADR of BACE1 by the ADR of Cerulean in each neuron (22). Since soluble cytoplasmic Cerulean distributes evenly throughout the neuron, an nADR equal to 1 indicates random distribution whereas an nADR greater than 1 indicates a preference for axonal targeting.

Statistical Analysis. Statistical analyses were performed using Prism 7 (GraphPad Software), and data are represented as mean ± SEM with the exception of Fig. 3 where the box plots represent the median and 25th/75th percentiles. Comparisons between two groups were performed by unpaired t tests or Mann–Whitney tests (two groups), and three or more groups were analyzed by ANOVA. ISF Aβ levels were analyzed by repeated measure two-way ANOVA. The Y-Maze test results were analyzed by ANOVA and also by z-normalization to allow for the comparison between different cohorts of animals.

1. Thinakaran G, Koo EH (2008) Amyloid precursor protein trafficking, processing, and function. *J Biol Chem* 283:29615–29619.
2. Mullan M, et al. (1992) A pathogenic mutation for probable Alzheimer's disease in the APP gene at the N-terminus of beta-amyloid. *Nat Genet* 1:345–347.
3. Citron M, et al. (1992) Mutation of the beta-amyloid precursor protein in familial Alzheimer's disease increases beta-protein production. *Nature* 360:672–674.
4. Cai XD, Golde TE, Younkin SG (1993) Release of excess amyloid beta protein from a mutant amyloid beta protein precursor. *Science* 259:514–516.
5. Di Fede G, et al. (2009) A recessive mutation in the APP gene with dominant-negative effect on amyloidogenesis. *Science* 323:1473–1477.
6. Jonsson T, et al. (2012) A mutation in APP protects against Alzheimer's disease and age-related cognitive decline. *Nature* 488:96–99.

Andrew et al.

7. Maloney JA, et al. (2014) Molecular mechanisms of Alzheimer disease protection by the A673T allele of amyloid precursor protein. *J Biol Chem* 289:30990–31000.
8. Kuhn PH, et al. (2012) Secretome protein enrichment identifies physiological BACE1 protease substrates in neurons. *EMBO J* 31:3157–3168.
9. Vassar R, et al. (2014) Function, therapeutic potential and cell biology of BACE proteases: Current status and future prospects. *J Neurochem* 130:4–28.
10. Vetrivel KS, et al. (2009) Alzheimer disease Abeta production in the absence of S-palmitoylation-dependent targeting of BACE1 to lipid rafts. *J Biol Chem* 284:3793–3803.
11. Linder ME, Deschenes RJ (2007) Palmitoylation: Policing protein stability and traffic. *Nat Rev Mol Cell Biol* 8:74–84.
12. Levental I, Grzybek M, Simons K (2010) Greasing their way: Lipid modifications determine protein association with membrane rafts. *Biochemistry* 49:6305–6316.
13. Hayashi T, Rumbaugh G, Huganir RL (2005) Differential regulation of AMPA receptor subunit trafficking by palmitoylation of two distinct sites. *Neuron* 47:709–723.
14. Lin DT, et al. (2009) Regulation of AMPA receptor extrasynaptic insertion by 4.1N, phosphorylation and palmitoylation. *Nat Neurosci* 12:879–887.
15. Hayashi T, Thomas GM, Huganir RL (2009) Dual palmitoylation of NR2 subunits regulates NMDA receptor trafficking. *Neuron* 64:213–226.
16. El-Husseini AE, et al. (2000) Dual palmitoylation of PSD-95 mediates its vesiculotubular sorting, postsynaptic targeting, and ion channel clustering. *J Cell Biol* 148:159–172.
17. Motoki K, et al. (2012) Neuronal β-amyloid generation is independent of lipid raft association of β-secretase BACE1: Analysis with a palmitoylation-deficient mutant. *Brain Behav* 2:270–282.
18. Drisdel RC, Green WN (2004) Labeling and quantifying sites of protein palmitoylation. *Biotechniques* 36:276–285.
19. Forrester MT, et al. (2011) Site-specific analysis of protein S-acylation by resin-assisted capture. *J Lipid Res* 52:393–398.
20. Vetrivel KS, et al. (2005) Spatial segregation of γ-secretase and substrates in distinct membrane domains. *J Biol Chem* 280:25892–25900.
21. Hitt B, et al. (2012) β-Site amyloid precursor protein (APP)-cleaving enzyme 1 (BACE1)-deficient mice exhibit a close homolog of L1 (CHL1) loss-of-function phenotype involving axon guidance defects. *J Biol Chem* 287:38408–38425.
22. Buggia-Prévot V, et al. (2014) Axonal BACE1 dynamics and targeting in hippocampal neurons: A role for Rab11 GTPase. *Mol Neurodegener* 9:1.
23. Rajapaksha TW, Eimer WA, Bozza TC, Vassar R (2011) The Alzheimer's β-secretase enzyme BACE1 is required for accurate axon guidance of olfactory sensory neurons and normal glomerulus formation in the olfactory bulb. *Mol Neurodegener* 6:88.
24. Cao L, Rickenbacher GT, Rodriguez S, Moulia TW, Albers MW (2012) The precision of axon targeting of mouse olfactory sensory neurons requires the BACE1 protease. *Sci Rep* 2:231.
25. Willem M, et al. (2006) Control of peripheral nerve myelination by the beta-secretase BACE1. *Science* 314:664–666.
26. Buxbaum JD, et al. (1998) Alzheimer amyloid protein precursor in the rat hippocampus: Transport and processing through the perforant path. *J Neurosci* 18:9629–9637.
27. Munro KM, Nash A, Pigoni M, Lichtenthaler SF, Gunnersen JM (2016) Functions of the Alzheimer's disease protease BACE1 at the synapse in the central nervous system. *J Mol Neurosci* 60:305–315.
28. Cirrito JR, et al. (2005) Synaptic activity regulates interstitial fluid amyloid-beta levels in vivo. *Neuron* 48:913–922.
29. Cirrito JR, et al. (2008) Endocytosis is required for synaptic activity-dependent release of amyloid-beta in vivo. *Neuron* 58:42–51.
30. Bero AW, et al. (2011) Neuronal activity regulates the regional vulnerability to amyloid-β deposition. *Nat Neurosci* 14:750–756.
31. Games D, et al. (1995) Alzheimer-type neuropathology in transgenic mice overexpressing V717F beta-amyloid precursor protein. *Nature* 373:523–527.
32. Johnson-Wood K, et al. (1997) Amyloid precursor protein processing and A beta42 deposition in a transgenic mouse model of Alzheimer disease. *Proc Natl Acad Sci USA* 94:1550–1555.
33. Zhao J, et al. (2007) Beta-site amyloid precursor protein cleaving enzyme 1 levels become elevated in neurons around amyloid plaques: Implications for Alzheimer's disease pathogenesis. *J Neurosci* 27:3639–3649.
34. Kandalepas PC, et al. (2013) The Alzheimer's β-secretase BACE1 localizes to normal presynaptic terminals and to dystrophic presynaptic terminals surrounding amyloid plaques. *Acta Neuropathol* 126:329–352.
35. Sadleir KR, et al. (2016) Presynaptic dystrophic neurites surrounding amyloid plaques are sites of microtubule disruption, BACE1 elevation, and increased Aβ generation in Alzheimer's disease. *Acta Neuropathol* 132:235–256.
36. Gowrishankar S, et al. (2015) Massive accumulation of luminal protease-deficient axonal lysosomes at Alzheimer's disease amyloid plaques. *Proc Natl Acad Sci USA* 112:E3699–E3708.
37. Buggia-Prévot V, et al. (2013) A function for EHD family proteins in unidirectional retrograde dendritic transport of BACE1 and Alzheimer's disease Aβ production. *Cell Rep* 5:1552–1563.
38. Buggia-Prévot V, Thinakaran G (2015) Significance of transcytosis in Alzheimer's disease: BACE1 takes the scenic route to axons. *Bioessays* 37:888–898.
39. Rivera JF, Ahmad S, Quick MW, Liman ER, Arnold DB (2003) An evolutionarily conserved dileucine motif in Shal K+ channels mediates dendritic targeting. *Nat Neurosci* 6:243–250.
40. Webster SJ, Bachstetter AD, Nelson PT, Schmitt FA, Van Eldik LJ (2014) Using mice to model Alzheimer's dementia: An overview of the clinical disease and the preclinical behavioral changes in 10 mouse models. *Front Genet* 5:88.
41. Ohno M, et al. (2006) Temporal memory deficits in Alzheimer's mouse models: Rescue by genetic deletion of BACE1. *Eur J Neurosci* 23:251–260.
42. Oakley H, et al. (2006) Intraneuronal beta-amyloid aggregates, neurodegeneration, and neuron loss in transgenic mice with five familial Alzheimer's disease mutations: Potential factors in amyloid plaque formation. *J Neurosci* 26:10129–10140.
43. Guilloux JP, Seney M, Edgar N, Sibille E (2011) Integrated behavioral z-scoring increases the sensitivity and reliability of behavioral phenotyping in mice: Relevance to emotionality and sex. *J Neurosci Methods* 197:21–31.
44. Janus C, Flores AY, Xu G, Borchelt DR (2015) Behavioral abnormalities in APPswe/PS1dE9 mouse model of AD-like pathology: Comparative analysis across multiple behavioral domains. *Neurobiol Aging* 36:2519–2532.
45. Zhu K, et al. (December 26, 2016) Beta-site amyloid precursor protein cleaving enzyme 1 inhibition impairs synaptic plasticity via seizure protein 6. *Biol Psychiatry*, 10.1016/j.biopsych.2016.12.023.
46. Blaskovic S, Blanc M, van der Goot FG (2013) What does S-palmitoylation do to membrane proteins? *FEBS J* 280:2766–2774.
47. Abrami L, Kunz B, Iacovache I, van der Goot FG (2008) Palmitoylation and ubiquitination regulate exit of the Wnt signaling protein LRP6 from the endoplasmic reticulum. *Proc Natl Acad Sci USA* 105:5384–5389.
48. Walker KR, Kang EL, Whalen MJ, Shen Y, Tesco G (2012) Depletion of GGA1 and GGA3 mediates postinjury elevation of BACE1. *J Neurosci* 32:10423–10437.
49. Ye X, et al. (2017) Regulation of synaptic amyloid-β generation through BACE1 retrograde transport in a mouse model of Alzheimer's disease. *J Neurosci* 37:2639–2655.
50. Lee EB, et al. (2005) BACE overexpression alters the subcellular processing of APP and inhibits Abeta deposition in vivo. *J Cell Biol* 168:291–302.
51. Koo EH, et al. (1990) Precursor of amyloid protein in Alzheimer disease undergoes fast anterograde axonal transport. *Proc Natl Acad Sci USA* 87:1561–1565.
52. Kang R, et al. (2008) Neural palmitoyl-proteomics reveals dynamic synaptic palmitoylation. *Nature* 456:904–909.
53. Thomas GM, Huganir RL (2013) Palmitoylation-dependent regulation of glutamate receptors and their PDZ domain-containing partners. *Biochem Soc Trans* 41:72–78.
54. Kaur I, et al. (2016) Activity-dependent palmitoylation controls SynDIG1 stability, localization, and function. *J Neurosci* 36:7562–7568.
55. El-Husseini Ael-D, Craven SE, Brock SC, Bredt DS (2001) Polarized targeting of peripheral membrane proteins in neurons. *J Biol Chem* 276:44984–44992.
56. Kanaani J, Diacovo MJ, El-Husseini Ael-D, Bredt DS, Baekkeskov S (2004) Palmitoylation controls trafficking of GAD65 from golgi membranes to axon-specific endosomes and a Rab5a-dependent pathway to presynaptic clusters. *J Cell Sci* 117:2001–2013.
57. Keith DJ, et al. (2012) Palmitoylation of A-kinase anchoring protein 79/150 regulates dendritic endosomal targeting and synaptic plasticity mechanisms. *J Neurosci* 32:7119–7136.
58. Thomas GM, Hayashi T, Chiu SL, Chen CM, Huganir RL (2012) Palmitoylation by DHHC5/8 targets GRIP1 to dendritic endosomes to regulate AMPA-R trafficking. *Neuron* 73:482–496.
59. Haass C, et al. (1995) The Swedish mutation causes early-onset Alzheimer's disease by beta-secretase cleavage within the secretory pathway. *Nat Med* 1:1291–1296.
60. Thinakaran G, Teplow DB, Siman R, Greenberg B, Sisodia SS (1996) Metabolism of the "Swedish" amyloid precursor protein variant in neuro2a (N2a) cells. Evidence that cleavage at the "β-secretase" site occurs in the golgi apparatus. *J Biol Chem* 271:9390–9397.
61. Yamamoto K, et al. (2015) Chronic optogenetic activation augments aβ pathology in a mouse model of Alzheimer disease. *Cell Reports* 11:859–865.
62. Cai Y, et al. (2012) BACE1 elevation is involved in amyloid plaque development in the triple transgenic model of Alzheimer's disease: Differential Aβ antibody labeling of early/preformed axon terminal pathology. *Neurotox Res* 21:160–174.
63. Cheng H, et al. (2009) S-palmitoylation of γ-secretase subunits nicastrin and APH-1. *J Biol Chem* 284:1373–1384.
64. Meckler X, et al. (2010) Reduced Alzheimer's disease ß-amyloid deposition in transgenic mice expressing S-palmitoylation-deficient APH1aL and nicastrin. *J Neurosci* 30:16160–16169.
65. Thinakaran G, Sisodia SS (1994) Amyloid precursor-like protein 2 (APLP2) is modified by the addition of chondroitin sulfate glycosaminoglycan at a single site. *J Biol Chem* 269:22099–22104.
66. Thinakaran G, et al. (1995) Distribution of an APP homolog, APLP2, in the mouse olfactory system: A potential role for APLP2 in axogenesis. *J Neurosci* 15:6314–6326.
67. Thinakaran G, et al. (1998) Stable association of presenilin derivatives and absence of presenilin interactions with APP. *Neurobiol Dis* 4:438–453.
68. Thinakaran G, et al. (1996) Endoproteolysis of presenilin 1 and accumulation of processed derivatives in vivo. *Neuron* 17:181–190.
69. Gong P, et al. (2011) Transgenic neuronal overexpression reveals that stringently regulated p23 expression is critical for coordinated movement in mice. *Mol Neurodegener* 6:87.
70. Rasband WS (1997–2016) ImageJ (Natl Inst Health, Bethesda), Version 1.51.